

1 **Infiltration effects on a two-dimensional molecular dynamics**  
2 **model of landslides**

3  
4 Authors: Gianluca Martelloni, Franco Bagnoli

5  
6 Gianluca Martelloni

7 Department of Energy Engineering and CSDC (Center of the Study of Complex  
8 System)

9 Via S. Marta 3, 50139 Firenze Italy

10 Corresponding author: Tel. +39 0554796592; fax: +39 0555609616

11 E-mail: gianluca.martelloni@unifi.it

12

13 Franco Bagnoli

14 Department of Energy Engineering and CSDC (Center of the Study of Complex  
15 System)

16 Via S. Marta 3, 50139 Firenze Italy

17 Also INFN, sez. Firenze

18 E-mail: franco.bagnoli@unifi.it

19

20 **Abstract:**

21 In this paper we propose a two-dimensional (2D) computational model, based on a  
22 molecular dynamics (MD) approach, for deep landslides triggered by rainfall. Our  
23 model is based on interacting particles or grains and describes the behavior of a  
24 fictitious granular material along a slope consisting of a vertical section, i.e. with a  
25 wide thickness. The triggering of the landslide is caused by the passing of two  
26 conditions: a threshold speed and a condition on the static friction of the particles, the  
27 latter based on the Mohr-Coulomb failure criterion (Coulomb 1776; Mohr 1914). The  
28 inter-particle interactions are through a potential that, in the absence of suitable  
29 experimental data and due to the arbitrariness of the grain dimension is modeled by  
30 means of a potential similar to the Lennard-Jones one (Lennard-Jones 1924), i.e., with  
31 an attractive and a repulsive part. For the updating of the particle positions we use a  
32 MD method which results to be very suitable to simulate this type of systems  
33 (Herrmann and Luding 1998). In order to take into account the increasing of the pore  
34 pressure due to the rainfall, a filtration model is considered. Finally we also introduce  
35 in the model the viscosity as a term in the dynamic equations of motion. The outcome

36 of simulations, from the point of view of statistical and dynamic characterization, is  
37 quite satisfactory relative to real landslides behavior and we can claim that this types  
38 of modeling can represent a new method to simulate landslides triggered by rainfall.

39

40 **Keywords:** Landslide; filtration model; molecular dynamics; computational technique

41

## 42 **1. Introduction**

43 Landslides are extreme and recurrent events in mountainous areas, often with many  
44 implications for urban environments, and consequently on the stricken population,  
45 with human casualties and economical losses (Van Asch et al., 2007). Major changes  
46 may be induced, sometimes, in a natural environment depending on the extent of the  
47 phenomenon. “A major threat is induced by all types of slope movements (e. g., falls,  
48 topples, slides, lateral spreads, flows)... which represent one of the most destructive  
49 natural hazards on earth” (Brabb 1991). For these reasons landsliding represents a  
50 challenging problem in Earth science. Often landslide triggering is caused by an  
51 intense and/or long rain. In particular, shallow landslides are triggered by short  
52 intense rainfalls (Campbell 1975; Crosta and Frattini 2007), while deep landslides are  
53 connected with prolonged and less intense rainfall events (Bonnard and Noverraz  
54 2001). Thanks to the rapid development of computers and advanced numerical  
55 methods, physical based models have been developed to predict the landslide  
56 triggering and to evaluate the run-out. Two fundamental approaches have been  
57 proposed to assess the dependence of landslide triggering on rainfall measurements.  
58 The first one relies on deterministic models (infiltration and geotechnical based) while  
59 the second defines the statistical rainfall thresholds above which the triggering of one  
60 or more landslides is possible (Segoni et al., 2009; Martelloni et al., 2011; Rosi et al.,  
61 2012). Regarding the propagation of a landslide, most of the numerical methods have  
62 used a continuum approach, i.e., an Eulerian point of view (Crosta et al. 2003, Patra et  
63 al. 2005). Other modeling approaches are based on cellular automata (Avolio et al.,  
64 2008). A relatively less common approach is the Lagrangian one, based on discrete-

65 particle methods, in which the material forming the slope (and the landslide) is  
66 represented as an ensemble of interacting elements, called particles or grains. The  
67 discrete element method (DEM) is used to model granular materials, debris flow and  
68 flow-like landslides (Cundall and Strack (1979); Iordanoff et al. 2010). Another  
69 Lagrangian method is the molecular dynamics (MD) one, closely related to DEM.  
70 This latter method is generally distinguished by the inclusion of rotational degrees-of-  
71 freedom as well as stateful contact and often complicated geometries. The inclusion of  
72 a more detailed description of the elementary components or their interactions and,  
73 above all, the increasing of the number of elements of the system allows for more  
74 realistic simulations, but the computational load can be very onerous. Obviously, the  
75 accuracy of the simulation has to be compared with the available experimental data.  
76 In the case of laboratory experiments, very accurate data can be obtained, but this is  
77 not possible for real landslides. These arguments motivated us to reduce the  
78 complexity of the model as much as possible, examining if this choice is compatible  
79 with the behavior of real landslides. In previous works we proposed a shallow  
80 landslide modeling (Massaro et al., 2011; Martelloni et al., 2012). In this paper we  
81 present an integration of a filtration model into a MD model for the starting and  
82 prosecution of particle movement along a slope, after a triggering induced by rainfalls.  
83 This model is conceived to be characteristic of deep landslides. The inclusion of the  
84 rainfall effect, i.e., the modeling of the effects due to the fluid that filters in the porous  
85 of the material, causing the landslide triggering, is a challenging problem. Our idea is  
86 to integrate the Iverson model of infiltration (Iverson, 2000) with the MD approach,  
87 by considering the infiltration at the particle level where we use a failure criterion of  
88 Mohr-Coulomb to assess the local triggering within the slope. Moreover we introduce  
89 in the model some stochastic variations to take into account the variability of the slope  
90 in terms of the water infiltration and frictional behavior. At present we do not pretend  
91 to be able to develop a model that simulates a real landslide or debris flow, rather we  
92 want to explore new alternative approache useful for this kind of problems. The  
93 resulting numerical method, similar to that of molecular dynamics (MD), is based on  
94 the use of an interaction potential between the particles, similar to the Lennard-Jones

95 one. As we shall see in the following sections, by means of this type of force we can  
96 also simulate a compressed state of the particles, according to a stress state of the  
97 slope material.

## 98 **2. Modeling approach**

### 99 **2.1 Filtration modeling and triggering mechanism**

100 In a previous work (Martelloni et al., 2012) we proposed a model for shallow  
101 landslides triggered by rainfall. This model is coarse-grained, based on fictitious  
102 particles, using a molecular dynamic approach for the update. In this previous version  
103 we considered only one particle layer. Due to this reason and to the quick response to  
104 rainfall of shallow landslide, we did not introduce there an infiltration model to  
105 integrate the triggering dynamics, although also for shallow landslides the triggering  
106 mechanism is related to pore pressure increasing. Obviously, in case of deep landslide  
107 this choice cannot be made and therefore we extended the model by including the  
108 crucial role of increasing pore pressure due to the rain infiltration, that is the main  
109 actor of the triggering mechanism (van Asch et al., 1999). At present we use the  
110 Iverson filtration model (Iverson 2000) that is adapted to the molecular dynamics  
111 approach according to the failure criterion of Mohr-Coulomb.

112 The idea is to use the one-dimensional infiltration equation along the  $z$  coordinate of  
113 the reference system ( $x$ - $z$ ) along the slope (Fig. 1):

$$114 \quad \frac{\partial \mu(z,t)}{\partial t} = K \cdot \frac{\partial^2 \mu(z,t)}{\partial z^2} \quad (1)$$

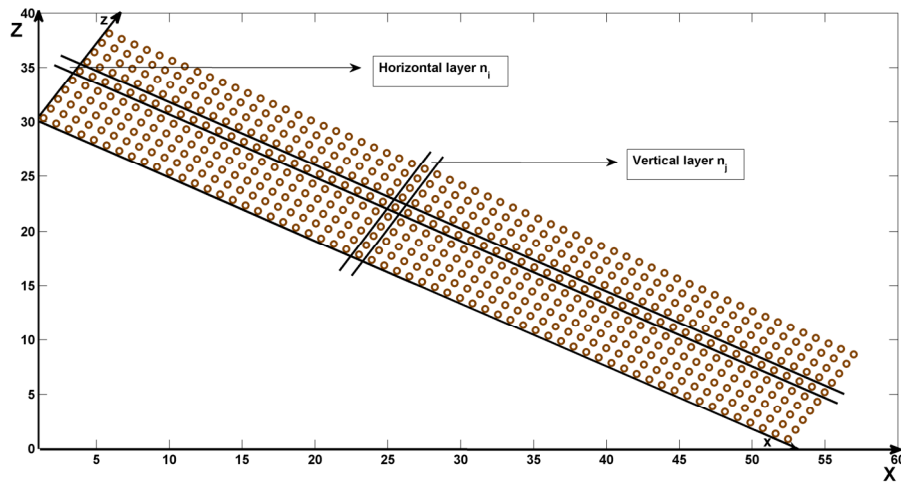
115 where  $\mu(z,t)$  is the pore pressure at depth  $z$  (in Eq. 1 the  $z$  coordinate is reverse with  
116 respect to Fig. 1) and time  $t$ , while  $K$  is the diffusion coefficient depending on slope  
117 angle  $\alpha$  that is held a constant in our simulations.

118 At the time  $t = 0$  the particles are arranged on a regular grid and the material is  
119 initially dry, i.e., it exhibits an initial pore pressure distribution equal to zero. Starting  
120 from time  $t = 0$ , a constant rain is simulated, but for each vertical layer  $n_j$  (Fig. 1) we  
121 assume a different infiltration (small stochastic variations) along  $x$  axes of the slope

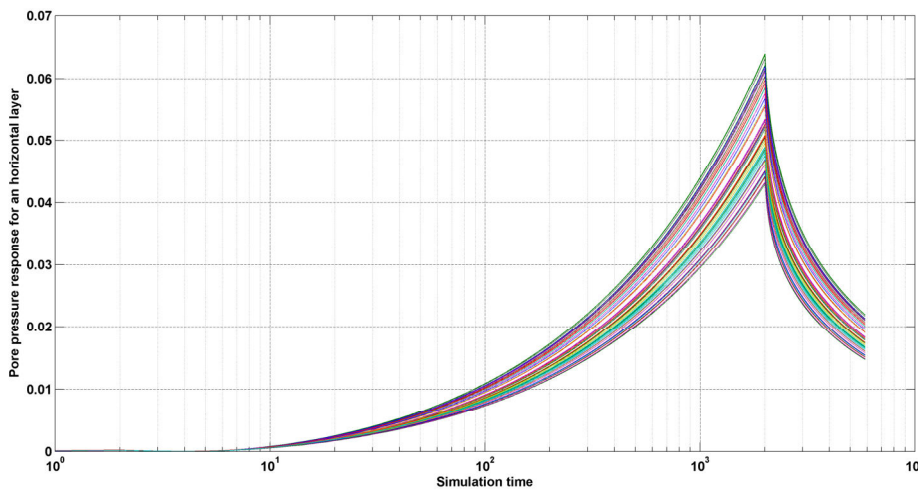
122 (Fig. 2). According to Eq. 1, the solution is given by the rainfall input per response  
 123 function, i.e.,

$$\begin{cases}
 \mu(z, t^*) = \frac{I_z}{K_z} \cdot R^* \\
 R^* = \begin{cases} R(t^*), & t^* \leq T^* \\ R(t^*) - R(t^* - T^*), & t^* > T^* \end{cases} \\
 R(t^*) = \sqrt{t^*/\pi} \cdot \exp(-1/t^*) - \operatorname{erfc}(1/\sqrt{t^*})
 \end{cases} \quad (2)$$

125 where  $t^*$  and  $T^*$  are respectively the normalized time and the normalized rainfall  
 126 duration (Iverson 2000), while  $I_z$  and  $K_z$  are respectively the average infiltration rate  
 127 and the hydraulic conductivity in the slope-normal direction.



128  
 129 **Figure 1** Reference system ( $x$ - $z$ ) of the slope modeled with particles arranged in a regular grid  
 130 according to disposition in horizontal and vertical layer



131  
 132 **Figure 2** The pore pressure response, in a simulation of our system, for each position  $x$  of a  
 133 horizontal layer  $n_i$  in the time steps of simulation: the differences are due to stochastic variations

134 Now let us show how the infiltration model is integrated into our numerical scheme  
 135 based on molecular dynamics (a discrete Lagrangian approach similar to DEM). The  
 136 first step is to appropriately relate the simulated rainfall with the water content of the  
 137 particles that constitute our fictitious soil. Let  $I_z$  be the discrete infiltration rate, i.e.,

$$138 \quad I_z = K_z \cdot \frac{\Delta h}{\Delta z} \quad (3)$$

139 We assume that  $\Delta h$  is the rainfall increment at a generic instant  $t$  and thickness  $z$ ,  
 140 while  $\Delta z$  is the initial distance between the centers of mass of two adjoining particles.  
 141 It is now possible to deduce  $I_z$  in terms of a mass ratio from simple considerations on  
 142 the density that can be expressed as:

$$143 \quad \rho = \frac{dm}{dV} = \frac{dm}{S \cdot dh} \quad (4)$$

144 where  $S$  is the unit area,  $m$  the mass and  $V$  the volume. Let us consider the density of  
 145 water  $\rho_w$  and the density of fictitious material (i.e. the particles)  $\rho_p$ . We obtain the  
 146 infinitesimal heights  $dh_w$  and  $dh_p$ ,

$$147 \quad \begin{cases} \rho_w = \frac{dm_w}{S_w \cdot dh_w} \Rightarrow dh_w = \frac{dm_w}{S_w \cdot \rho_w} \\ \rho_p = \frac{dm_p}{S_p \cdot dh_p} \Rightarrow dh_p = \frac{dm_p}{S_p \cdot \rho_p} \end{cases} \quad (5)$$

148 but, in our case, since the dimensions of particles are relatively small, it is possible to  
 149 consider, to a good approximation,

$$150 \quad S_w \cdot \rho_w = S_p \cdot \rho_p \quad (6)$$

151 Consequently, the ratio between  $dh_w$  and  $dh_p$  gives the new discrete infiltration rate  $I_z$ :

$$152 \quad \left\{ \frac{dh_w}{dh_p} = \frac{dm_w}{dm_p} \Rightarrow \frac{\Delta h_w}{\Delta h_p} = \frac{\Delta m_w}{\Delta m_p} \Rightarrow I_z = K_z \cdot \frac{\Delta m_w}{\Delta m_p} \right. \quad (7)$$

153 Hence, we can simulate the rainfall in terms of water mass and, using the response  
 154 function  $R^*$ , we can take into account the absorbed water in time and space at  
 155 thickness  $z$ , i.e., at each level of the particle layers.

156 Consequently, since the gravity acts on each particle  $i$ , its components can be  
 157 expressed along the slope reference system as:

$$158 \quad \mathbf{F}_{gi} = \{g \cdot \sin(\alpha) \cdot [m_i + w_i(t)], -g \cdot \cos(\alpha) \cdot [m_i + w_i(t)]\} \quad (8)$$

159 where  $g$  is the gravity acceleration,  $\alpha$  the angle of the slope,  $m_i$  is the dry mass,  
 160 variable from particle to particle and  $w_i(t)$  is the cumulative absorbed water in time.  
 161 The interaction force  $\mathbf{F}_{ij}$ , that acts on particle  $i$  due to particle  $j$ , is defined trough a  
 162 potential inspired to the Lennard-Jones one, i.e., we consider that the repulsive and  
 163 attractive term of the potential or force are weighted differently:

$$\mathbf{F}_{ij} = -\mathbf{F}_{ji} = -\left[ k_1 \left( \frac{r}{R_{ij}} \right)^{-2} - k_2 \left( \frac{r}{R_{ij}} \right)^{-1} \right] \cdot \hat{\mathbf{r}}$$

$$164 \quad R_{ij} = L = 1 \quad (9)$$

$$r = |\mathbf{r}_{ij}| = \sqrt{(x_j - x_i)^2 + (y_j - y_i)^2}$$

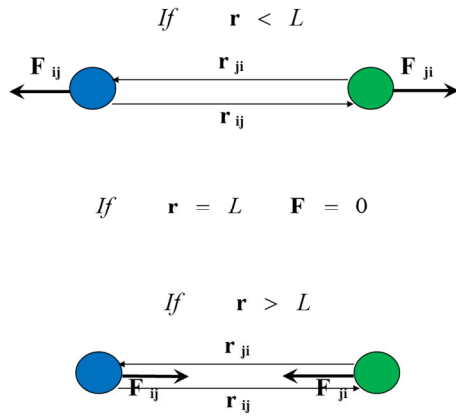
165 where  $r$  is the distance between the centers of mass,  $k_1$  and  $k_2$  are constants ( $k_1 = k_2$  in  
 166 “classical” Lennard-Jones potential),  $\hat{\mathbf{r}}$  is the unit vector relative to the force and  $L$  is  
 167 the equilibrium distance (Fig. 3). If  $k_1 = k_2$  we have the equilibrium at distance  $L = 1$   
 168 (Fig. 4), else if  $k_1 \neq k_2$  it is possible simulate, starting from  $t = 0$ , a compressed stress  
 169 state of the particles (Fig. 5). The justification of such interaction force is due  
 170 simulation results that are similar to real landslide behavior (see simulations section).  
 171 As mentioned previously, at instant  $t = 0$  the system is prepared in equilibrium, that is,  
 172 the particles are disposed on a regular grid (Fig. 1). Therefore, as triggering  
 173 mechanism, we consider the law of Mohr-Coulomb (Coulomb 1776; Mohr 1914) in  
 174 the form of the effective stress (Terzaghi 1943),

$$175 \quad \tau_f = (\sigma - \mu) \cdot \tan \phi' + c' \quad (10)$$

176 where  $\tau_\phi$  is the shear stress at failure,  $\sigma$  the normal stress,  $\phi'$  the friction angle and  $c'$   
 177 the cohesion term. As the Mohr-Coulomb failure criterion is a simple friction law,  
 178 short of the term of cohesion, it can be easily adapted to our case, rewriting Eq. (10)  
 179 as follows:

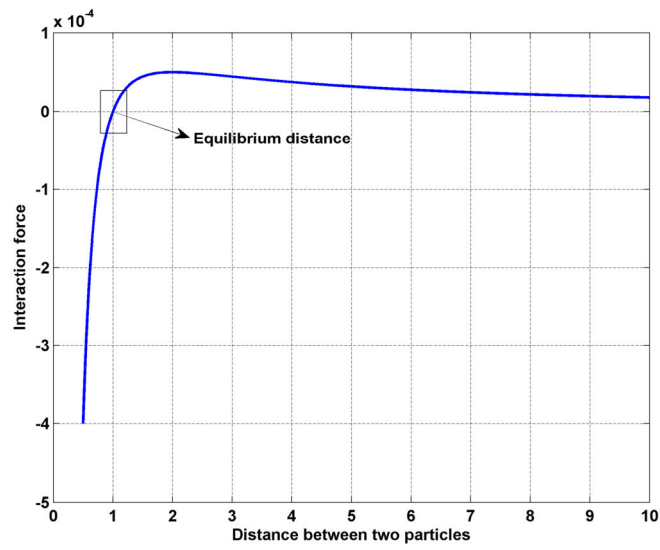
$$180 \quad \tau_f = F_s + c' = [M(z, t) \cdot g \cdot \cos(\alpha) - \mu(z, t)] \cdot \mu_s + c' \quad (11)$$

181 where  $M$  is the term  $m_i + w_i(t)$ , relative to particle  $i$ , considered in Eq. (8). Note that  
 182 varying the thickness  $z$ , the considered particle layer differs due to the discreteness of  
 183 the system.



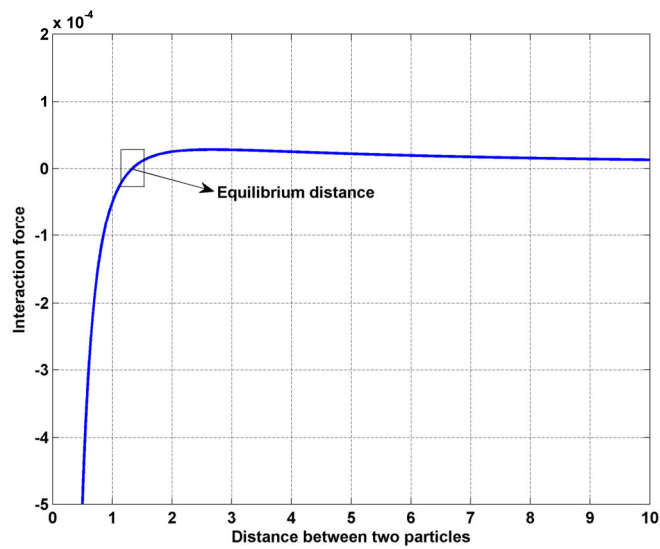
184

185 **Figure 3** Schematic description of the interaction force



186

187 **Figure 4** Interaction force for the equilibrium distance  $L = 1$



188

189 **Figure 5** Interaction force for the equilibrium distance  $L > 1$  (simulated initial compressed stress  
190 state)

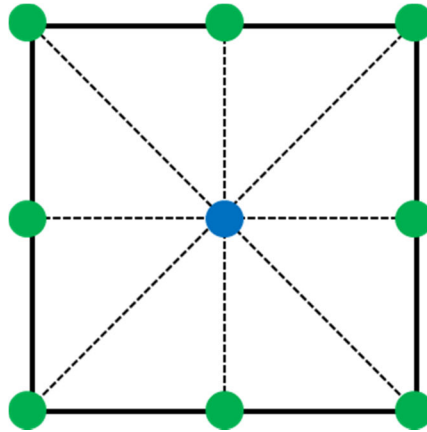


191 Finally, in our model, we express the local triggering, i.e., the triggering at the particle  
 192 level, using a failure criterion and considering a speed threshold  $v_d$  for the static-  
 193 dynamic transition. In synthesis, for each particle  $i$ :

$$194 \begin{cases} |\mathbf{F}_i| < F_{si} + c'_i \\ |\mathbf{v}_i| < v_d \end{cases} \quad (12)$$

$$195 \mathbf{F}_i = \mathbf{F}_{gi} + \sum_{j=1}^{n_k} \mathbf{F}_{ij} \quad (13)$$

196 where  $|\mathbf{F}_i|$  represents the module of the active forces, i.e., the force of gravity  $\mathbf{F}_{gi}$  plus  
 197 the force resulting from the potential, the latter being the sum of terms in Eq. (13)  
 198 where  $n_k$  denote the total number of particles among the next-to-nearest neighbors in  
 199 interaction with particle  $i$ , i.e., for initial instant,  $n_k = 8$  (Fig. 6), while  $|\mathbf{v}_i|$  is the  
 200 module of the speed. This double control, expressed by Eqs. (12) on the forces and  
 201 velocity, permits both the triggering and the stopping of the particle motion.



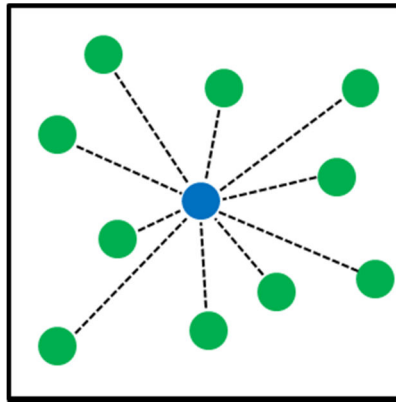
202  
 203 **Figure 6** Interaction, at instant  $t = 0$  for each particle of the system, according to second neighbors  
 204 one

## 205 2.2 Dynamics condition and updating algorithm

206 Eqs. (12) are valid in dynamical conditions, as they represent, in synthesis, a control  
 207 on the state of motion of the particles. Once a particle is moving, we consider also, as  
 208 active force, a dynamic friction (the force direction is opposed to the velocity one),  
 209 expressed for each particle  $i$  by:

$$210 \mathbf{F}_{di} = (m_i + w_i(t))g \cos(\alpha) \cdot (\mu_d \cdot \exp(-w_0 t) + \mu_{dlow} \cdot (1 - \exp(-w_0 t))) \cdot (-\hat{\mathbf{v}}) \quad (14)$$

211 The force in Eq. (14) depends on two friction terms, characterized by coefficients  $\mu_d$   
 212 and  $\mu_{dlow}$ , i.e.  $\mu_d$  for  $t = 0$  and  $\mu_{dlow}$  for  $t \rightarrow \infty$ , with  $\mu_d > \mu_{dlow}$ . In synthesis, the effect of  
 213 rainfall is to decrease the friction of the particles during time (through the constant  
 214 velocity  $w_0$  of the exponential). Moreover the friction coefficients  $\mu_d$  and  $\mu_{dlow}$  vary  
 215 randomly (with a small dispersion) with the position, modeling the roughness between  
 216 the particles. This friction law is inspired by Jop et al. (2006).  
 217 As previously mentioned, initially the particles are arranged on a regular grid, i.e., at  
 218 the instant  $t = 0$  each mass is placed in the nodes of a regular rectangular grid and  
 219 therefore every particle interacts with the eight blocks placed in the nearest and next-  
 220 to-nearest nodes (Fig. 6). At each time step, the interactions are re-calculated for each  
 221 object within a given interaction range. This technique is used in molecular dynamics  
 222 and congruent with principle of action and reaction (Fig. 7).



223  
 224 **Figure 7** Ri-calculus of interaction for each mass within the assigned range

225 Generally, in MD and accordingly in our simulations, the updating of the positions  
 226 and velocities is based on the first or second-order Verlet algorithm (Verlet 1967).  
 227 The latter is very stable, allowing a good numerical approximation. Moreover, as the  
 228 forces are calculated once for each time step, this computational updating method  
 229 does not require a large computational power.  
 230 When a mass is moving, the total force  $\mathbf{F}$  that acts on it is given by the sum of the  
 231 active forces, the dynamic friction force and a term of viscosity with coefficient  $\mu$ ,

232 
$$\mathbf{F} = \mathbf{F}_i + \mathbf{F}_{di} + \mathbf{F}_{\gamma i} = \mathbf{F}_{gi} + \sum_{j=1}^{j=n_k} \mathbf{F}_{ij} + \mathbf{F}_{di} - \mu \cdot \mathbf{v}_i \quad (15)$$

233 In this case, the value  $n_k$  in the sum of Eq. (15) can be less or grather than 8, due to the  
234 possible compression effects during the motion of masses.

235 The velocity Verlet algorithm, for the updating of positions  $\mathbf{r}$  and velocities  $\mathbf{v}$  of each  
236 particles between two instant of difference  $\Delta t$ , reads

$$237 \begin{cases} \mathbf{r}(t + \Delta t) = \mathbf{r}(t) + \mathbf{v}(t)\Delta t + \frac{\mathbf{F}(t)}{m} \Delta t^2 \\ \mathbf{v}(t + \Delta t) = \mathbf{v}(t) + \frac{1}{2m} [\mathbf{F}(t + \Delta t) + \mathbf{F}(t)]\Delta t \end{cases} \quad (16)$$

238 Summing up we note that, in the case of uniform rainfall, it is simple to theoretically  
239 deduce the time of local triggering, i.e., the time of the first particle detachment.

240 However, since the sliding masses could stop after a first detachment, the triggering of  
241 single particle cannot represent the definition of landslide triggering. A better  
242 definition in this sense is based on the motion of center of mass of the global system  
243 or the center of mass of all particle in motion (Martelloni et al. 2012). In the next  
244 section we see that is possible to use a Fukuzono method (Fukuzono 1985) to predict  
245 the failure time for our simulated system.

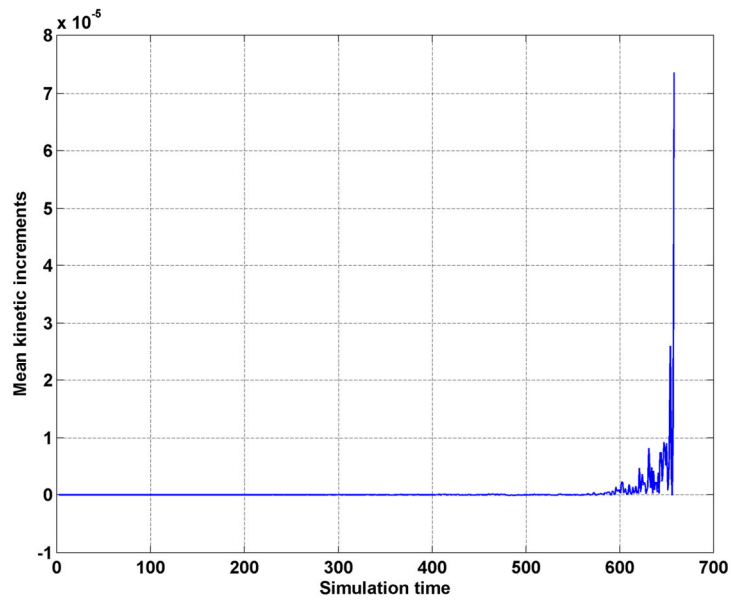
### 246 **3. Results of model simulations**

247 In this section we show the simulation results, and exhibit some peculiarities that  
248 emerge from the analysis of generated data. Regarding the dynamics, we observe the  
249 typical stick-and-slip dynamics of frictional systems, earthquake faults and landslides  
250 (Nielsen et al., 2010) that is also observed in other MD model as the seismic fault one  
251 (Ciamarra et al., 2010). In Figs. 8 and 9 the mean kinetics increment of the particles  
252 and the mean velocity are reported, respectively. It is possible to note a first stick  
253 phase and a subsequent slip one (Heslot et al., 1994). In Fig. 10, the time behavior of  
254 the inverse of the mean velocity is plotted and there we can note better the initial stick  
255 phase. The behavior of this simulation, in terms of the velocity, is similar to real  
256 landslide (Suwa et al., 2010). As mentioned above, we use the Fukozono method of  
257 the inverse of velocity for the evaluation of failure time of simulated landslide. Let us  
258 apply first this method to the initial part of the simulation, corresponding to the  
259 maximum slope of the inverse of velocity (green circle in Fig. 11) up to consider all

260 the points (red circle in Fig. 11), evaluating the time of triggering by means of the  
261 calibration function,

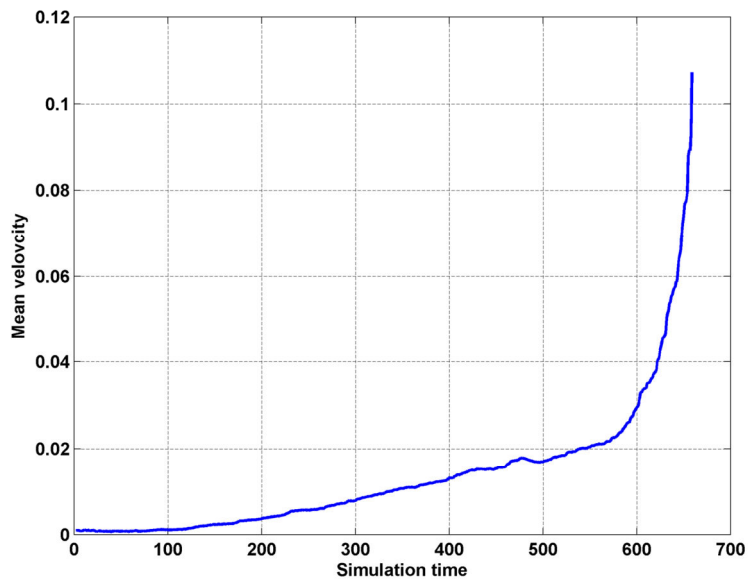
$$262 \quad \frac{1}{v} = [\beta \cdot (\alpha - 1)]^{\frac{1}{\alpha-1}} \cdot (t_r - t)^{\frac{1}{\alpha-1}} \quad (17)$$

263 where  $v$  is the mean velocity of the simulated landslide (i.e., the masses in motion),  $t$   
264 the time of simulation,  $t_r$  the time of failure, while  $\alpha$  and  $\beta$  are constant. These  
265 evaluated triggering times vary from 150 to 220 simulation time steps.



266

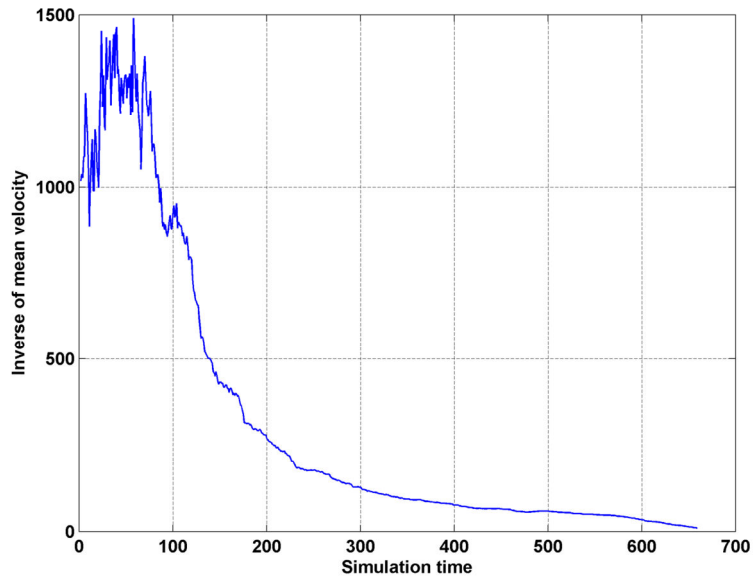
267 **Figure 8** Mean kinetic increment versus simulation time



268

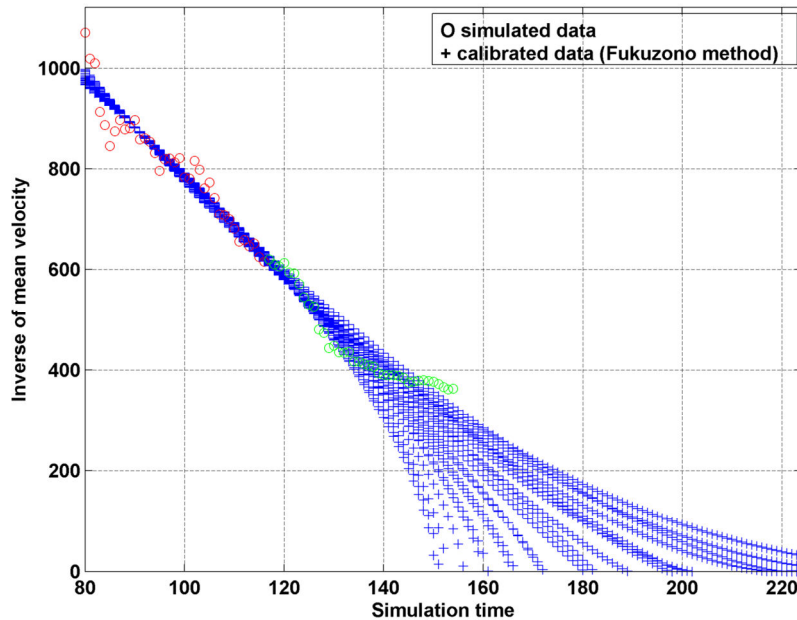
269 **Figure 9** Mean velocity versus simulation time

270



271

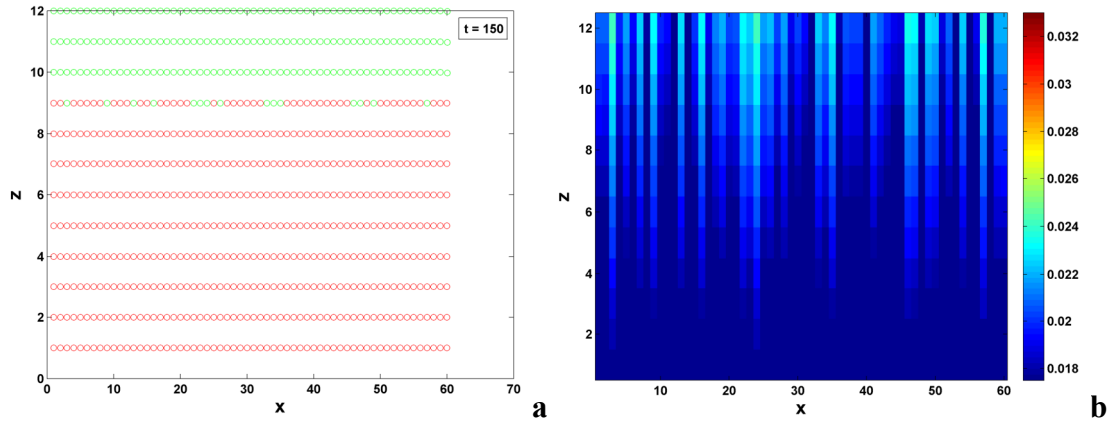
272 **Figure 10** Inverse of mean velocity versus simulation time



273

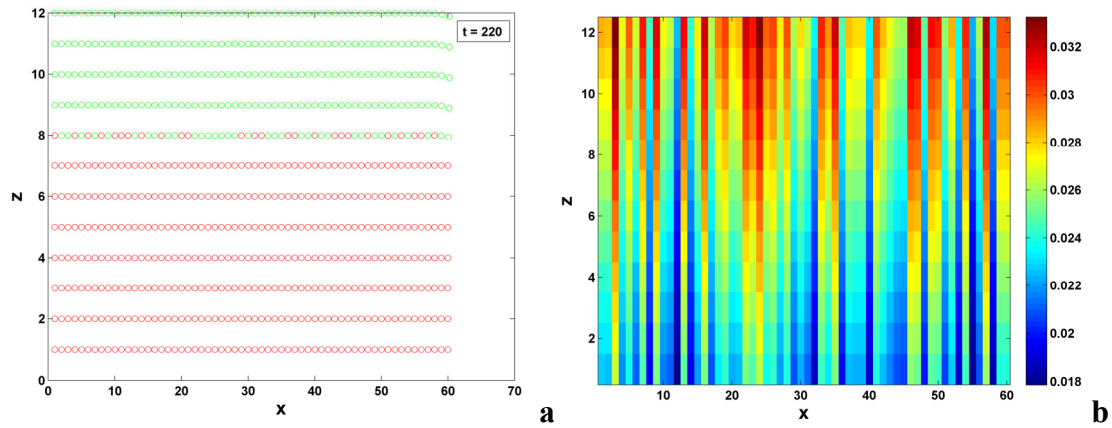
274 **Figure 11** Application of the inverse velocity method (Fukuzono 1985) to our simulated system

275 In Figs. 12(a) and 13(a) the landslide configuration is reported in the coordinate  
 276 system of the slope ( $x$ - $z$ ) for the extreme values of the evaluated range of time  
 277 triggering. We observe an initial motion of the upper horizontal layer and an initial  
 278 phase of creep (in the system representation the green particles are in motion, while  
 279 the red ones are at rest). In Figs. 12(b) and 13(b), the infiltration states for each  
 280 position of slope are reported for  $t = 150$  and  $t = 220$ . Moreover, in Fig. 14 we report a  
 281 system configuration of the same simulation at  $t = 600$  where we note a slip phase  
 282 with creep, detachments and arching phenomena.



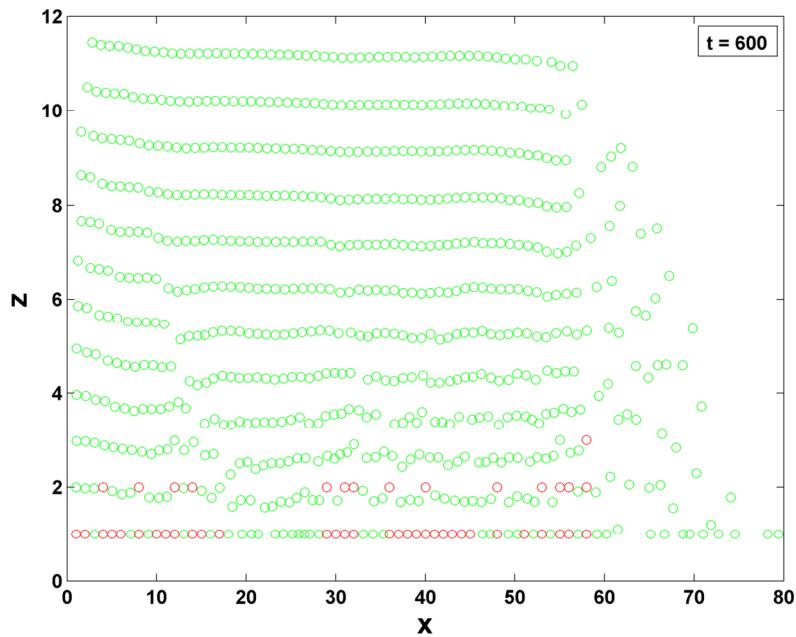
283

284 **Figure 12 (a)** The simulated landslide in the coordinate system of the slope for  $t = 150$  **(b)** The  
 285 simulated infiltration along the slope for  $t = 150$



286

287 **Figure 13 (a)** The simulated landslide in the coordinate system of the slope for  $t = 220$  **(b)** The  
 288 simulated infiltration along the slope for  $t = 220$



289

290 **Figure 14** The simulated landslide in the coordinate system of the slope for  $t = 600$

291 Other interesting results can be observed from a statistical point of view (Martelloni et  
292 al., 2012): we perform some simulations varying the viscosity coefficient  $\mu$  of Eq. 15.  
293 We observe a transition of the mean energy increment distribution from Gaussian to  
294 power law after decreasing the viscosity coefficient from a finite initial value up to  
295 zero, as shown in Figs. 15, 16 and 17. This behavior is compatible with the  
296 corresponding velocity increasing of the landslide after decreasing the viscosity. In  
297 other words, this behavior is congruent with the stick-and-slip dynamics. Thus, the  
298 transition of the mean energy increment distribution is also observed in the same  
299 simulation at different times, i.e., by calculating this distribution in stick phase we  
300 observe a Gaussian distribution and not a power law even for a viscosity coefficient  $\mu$   
301  $= 0$ , while considering the distribution in the slip phase we observe a power law also  
302 for high viscosity. Finally, we measured the time interval between successive time  
303 steps of the simulation ( $t, t+I$ ) for which the masses start to move, i.e., we observe the  
304 distribution of the subsequent local triggering. In all simulations a power law  
305 distribution is observed (see in Fig. 18 the obtained result for  $\mu = 0$ ). Finally in Tables  
306 1 and 2 we reported the adopted fit estimators (Eqs. 21) and the optimal fit parameters  
307 ( $a_1, b_1, c_1, a, b$ ) of the obtained distributions according to Eqs. 18, 19 and 20, i.e.,  
308 Gaussian, log-normal and power law, respectively:

$$309 \quad f(x) = a_1 \cdot \exp\left(-\left(\frac{x-b_1}{c_1}\right)^2\right) \quad (18)$$

$$310 \quad f(x) = a \cdot \exp(b) \quad (19)$$

$$311 \quad f(x) = a \cdot x^b \quad (20)$$

312 where  $x$  is the analyzed data.

313 The adopted estimators of the fitting accuracy are,

$$SSE = \sum_{i=1}^n (y_i - \hat{y}_i)^2$$

$$R^2 = 1 - \frac{SSE}{SST}; \quad SST = \sum_{i=1}^n (y_i - \bar{y}_i)^2$$

314

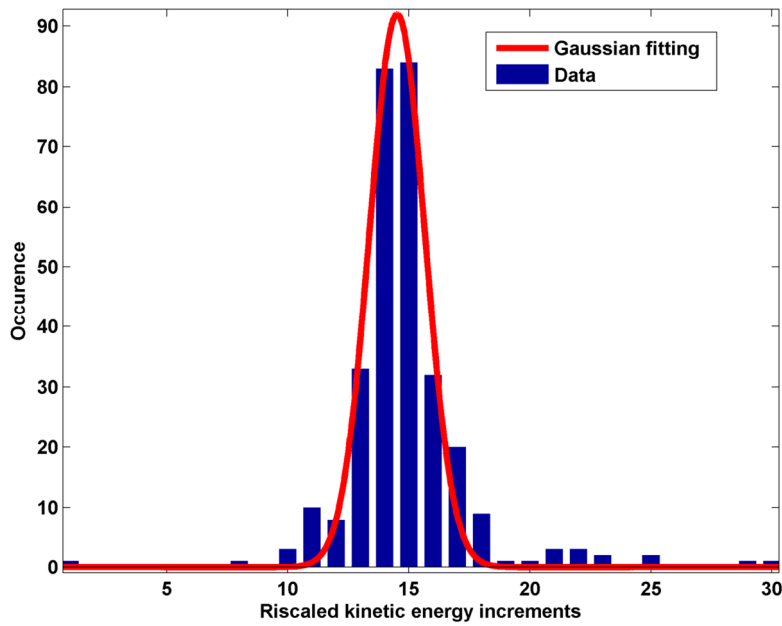
$$\hat{R}^2 = 1 - (1 - R^2) \frac{n-1}{n-p-1}$$

$$RMSE = \sqrt{\frac{SSE}{n-m}}$$

(21)

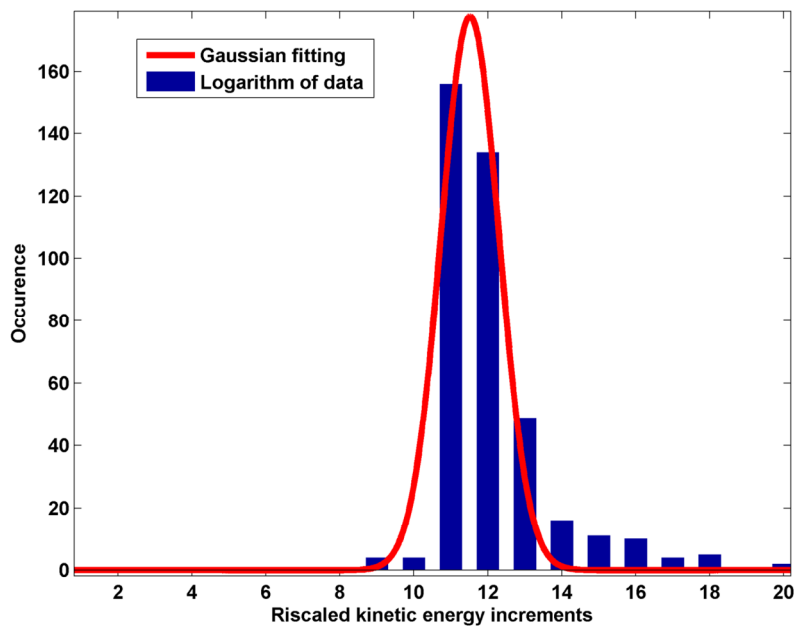
315 i.e., *SSE* is the *Sum of Squared Residuals*,  $R^2$  is the *Coefficient of Determination*,  $\hat{R}^2$  is

316 *R Bar Squared* and *RMSE* is the *Root Mean Square Error*.



317

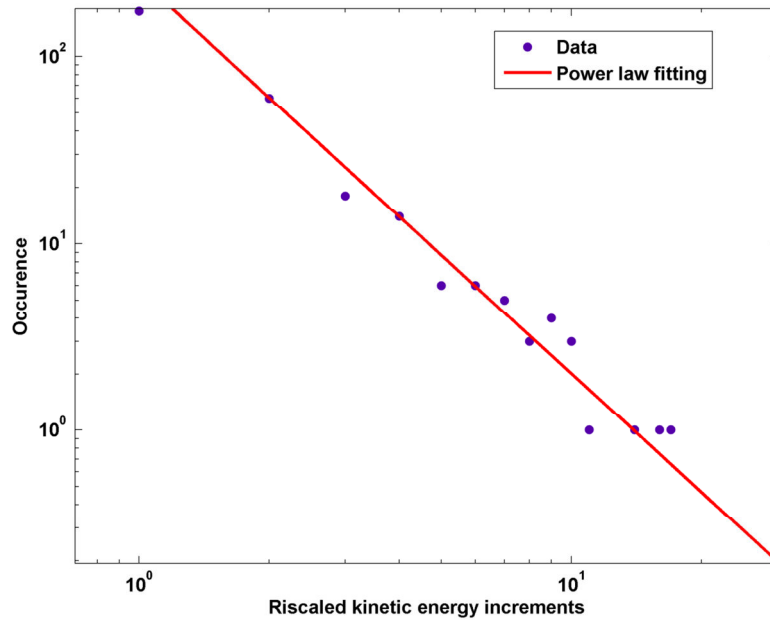
318 **Figure 15** The distribution of kinetic energy increments for  $\mu = 0.01$



319

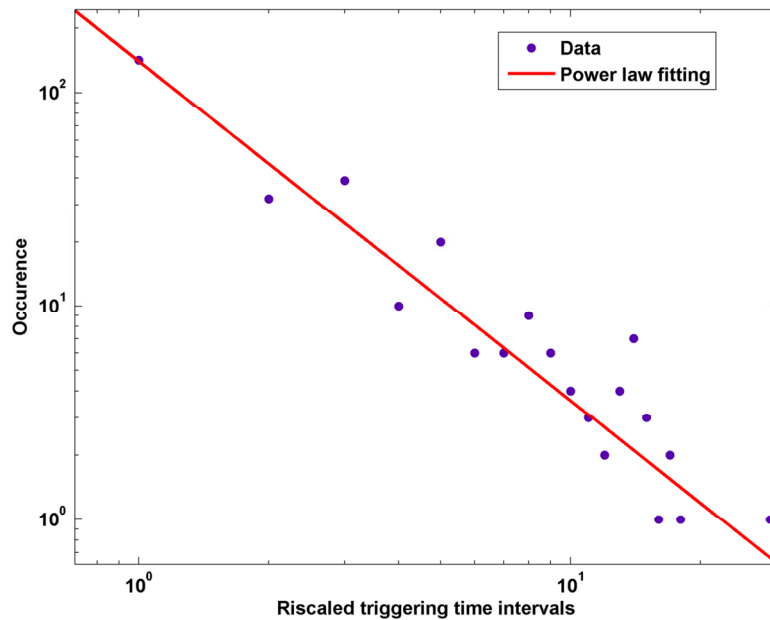
320 **Figure 16** The distribution of kinetic energy increments for  $\mu = 0.0025$





321

322 **Figure 17** The distribution of kinetic energy increments for  $\mu = 0$



323

324 **Figure 18** The distribution of triggering time intervals for  $\mu = 0$

325 **Table 1** Kinetic energy increment distribution varying the coefficient of viscosity  $\mu$ , parameters of  
 326 fit goodness and parameters of obtained distribution

$\mu$ (Distribution)	0.01 (Gaussian)	0.0025 (Log-Normal)	0 (Power law)	
SSE	131.9	1752		
R-Square	0.9904	0.9531	SSE	32.52
Adjusted-R-Square	0.9897	0.9475	R-Square	0.999
RMSE	2.21	10.15	Adjusted-R-Square	0.9989
$a_1$	91.94	177.4	RMSE	1.078
$b_1$	14.52	11.52	a	259.1
$c_1$	1.612	1.108	b	-2.11

327

328 **Table 2** Local time triggering distribution varying the coefficient of viscosity  $\mu$ , parameters of fit  
 329 goodness and parameters of obtained power law distribution

$\mu$ (Distribution)	0.01 (Power law)	0.0025 (Power law)	0 (Power law)
SSE	238.3	206.1	602.7
R-Square	0.9973	0.9936	0.9706
Adjusted-R-Square	0.9972	0.9933	0.9696
RMSE	2.917	2.713	4.639
a	353.1	174.4	139.9
b	-1.722	-1.469	-1.59

330

#### 331 **4. Discussion and conclusions**

332 In our opinion though the model proposed in this paper is still quite schematic, our  
 333 results encourage for the researche in this direction. The results are consistent with the  
 334 behavior of real landslides induced by rainfall and an interesting behavior emerges  
 335 from the dynamic and statistical points of view. Emerging phenomena such as  
 336 fractures, detachments and arching can be observed. In particular, the model  
 337 reproduces well the energy and time distribution of avalanches, analogous to the  
 338 observed Gutenberg-Richter and Omori power law distributions for earthquakes  
 339 (Gutenberg and Richter 1956; Omori 1895). We note that other natural hazards  
 340 (landslides, earthquakes and forest fires) also exhibit a power law distribution  
 341 (Malamud et al., 2004; Turcotte 1997), characteristic of self-organized critical  
 342 systems (Turcotte and Malamud 2004). Moreover, we observed an interesting  
 343 statistical characteristic of this type of systems, i.e., a transition of the mean energy  
 344 increment distribution from Gaussian to power law after decreasing the viscosity  
 345 coefficient up to zero. This behavior is compatible with the corresponding velocity  
 346 increase. The main advantage of these Lagrangian methods consists in the capability  
 347 of following the trajectory of a single particle, possibly identifying its dynamical  
 348 properties. Actually, we observed a characteristic velocity and energy pattern typical  
 349 of a stick-and-slip dynamics, similar to real landslides behavior (Sornette et al., 2004).  
 350 Moreover, we have shown that it is possible to apply the method of the inverse  
 351 surface displacement velocity for predicting the failure time (Fukuzono 1985).

## 352 **Acknowledgements**

353 We thank the Ente Cassa di Risparmio di Firenze for its support under the contract  
354 *Studio dei fenomeni di innesco e propagazione di frane in relazione ad eventi di*  
355 *pioggia e/o terremoti per mezzo di modelli matematici ed esperimenti di laboratorio*  
356 *su mezzi granulari.*

## 357 **References**

- 358 Avolio MV, Lupiano V, Mazzanti P, Di Gregorio S (2008) Modelling combined subaerial-  
359 subaqueous flow-like landslides by Macroscopic Cellular Automata. In: Umeo H et al. (ed)  
360 ACRI 2008, LNCS 5191: 329–336
- 361 Bonnard CH, Noverraz F (2001) Influence of climate change on large landslides: assessment of  
362 long term movements and trends. In: Proceedings of the International Conference on  
363 Landslides causes impact and countermeasures. Gluckauf, Essen, Davos, 121–138
- 364 Brabb EE (1991) The world landslide problem. Episodes, 14: 52-61
- 365 Campbell R (1975) Soil slips, debris flows and rainstorms in the Santa Monica Mountains and  
366 vicinity, Southern California. USGS Professional Paper, 851: 51 pp
- 367 Ciamarra MP, Lippiello E, Godano C, de Arcangelis L (2010) Unjamming Dynamics: The  
368 Micromechanics of a Seismic Fault Model. Physical Review Letters 104, 23800, DOI:  
369 10.1103/PhysRevLett.104.238001
- 370 Coulomb CA (1776) Essai sur une application des regles des maximis et minimis a quelques  
371 problemes de statique relatifs, a la architecture. Mem. Acad. Roy. Div. Sav., 7: 343-387
- 372 Crosta GB, Imposimato S, Roddeman DG (2003) Numerical modelling of large landslides  
373 stability and runout. Natural Hazards and Earth System Science 3(6): 523-538
- 374 Crosta GB, Frattini P (2007) Rainfall-induced landslides and debris flows. Hydrol. Process., 22:  
375 473–477
- 376 Cundall PA, Strack ODL (1979) A discrete numerical model for granular assemblies.  
377 Geotechnique 29(819): 47-65
- 378 Fukuzono T (1985) A new method for predicting the failure time of a slope. Proc. 4th Int. Conf.  
379 Field Workshop Landslides, 145–150. Tokyo: Jpn. Landslide Soc.
- 380 Gutenberg B, Richter CF (1956) Magnitude and energy of earthquakes. Ann. Geofis., 9(1)
- 381 Herrmann HJ, Luding S (1998) Modeling granular media on the computer. Continuum Mech.  
382 Thermodyn., 10: 189-231
- 383 Heslot F, Baumberger T, Perrin B, Caroli B, Caroli C (1994) Creep, stick-slip, and dry-friction  
384 dynamics: Experiments and a heuristic model. Physical Review E 49: 6
- 385 Iordanoff I, Iliescu D, Charles JL, Neauport J (2010) Discrete element method, a tool to  
386 investigate complex material behaviour in material forming. AIP Conference Proceedings,  
387 1252(1): 778–786, doi: 10.1063/1.3457634, URL <http://link.aip.org/link/?APC/1252/778/1>.
- 388 Iverson RM (2000) Landslide triggering by rain infiltration. Water Resources Research 36(7):  
389 1897-1910
- 390 Jop P, Forterre Y, Pouliquen O (2006) A constitutive law for dense granular flows. Nature 441:  
391 727-730

392 Lennard-Jones J E (1924) On the Determination of Molecular Fields. Proc. R. Soc. Lond. A, 106  
393 (738): 463–477

394 Malamud BD, Turcotte DL, Guzzetti F, Reichenbach P (2004) Landslide inventories and their  
395 statistical properties. *Earth Surface Processes and Landforms*, 29: 687-711

396 Martelloni G, Segoni S, Fanti R, Catani F (2011) Rainfall thresholds for the forecasting of  
397 landslide occurrence at regional scale. *Landslides* DOI: 10.1007/s10346-011-0308-2

398 Martelloni G, Massaro M, Bagnoli F (2012) A computational toy model for shallow landslides:  
399 Molecular Dynamics approach. arXiv: 1208.6116v1 [physics.geo-ph]

400 Massaro E, Martelloni G, Bagnoli F (2011) Particle based method for shallow landslides:  
401 modeling sliding surface lubrication by rainfall. *CMSIM International Journal of Nonlinear*  
402 *Scienze* ISSN 2241-0503, 147-158

403 Mohr O (1914) *Abhandlungen aus dem Gebiete der Technischen Mechanik* (2nd ed). Ernst, Berlin

404 Nielsen S, Taddeucci J, Vinciguerra S (2010) Experimental observation of stick-slip instability  
405 fronts. *Geophysical Journal International*, 180: 697–702

406 Omori F (1895) On the aftershocks of earthquakes. *J. Coll. Sci. Imp. Univ. Tokyo*, 7: 111-200

407 Patra AK, Bauer AC, Nichita CC, Pitman EB, Sheridan MF, Bursik M, Rupp B, Webber A,  
408 Stinton A, Namikawa L, Renschler C (2005) Parallel adaptive numerical simulation of dry  
409 avalanches over natural terrain. *Journ. of Volc. and Geot. Res.*, 139: 1-21

410 Rosi A, Segoni S, Catani F, Casagli N (2012) Statistical and environmental analyses for the  
411 definition of a regional rainfall threshold system for landslide triggering in Tuscany (Italy). *J.*  
412 *Geogr. Sci.* 22(4): 617-629

413 Segoni S, Leoni L, Benedetti AI, Catani F, Righini G, Falorni G, Gabellani S, Rudari R, Silvestro  
414 F, Reborà N (2009) Towards a definition of a real-time forecasting network for rainfall  
415 induced shallow landslides. *Natural Hazards and Earth System Sciences*, 9: 2119-2133

416 Sornette D, Helmstetter A, Grasso JR, Andersen JV, Gluzman S, Pisarenko V (2004) Towards  
417 Landslide Predictions: Two Case Studies. *Physica A*, 338: 605-632

418 Suwa H, Mizuno T, Ishii T (2010) Prediction of a landslide and analysis of slide motion with  
419 reference to the 2004 Ohto slide in Nara, Japan. *Geomorphology* 124: 157-163

420 Terzaghi K (1943) *Theoretical soil mechanics*. New York: Wiley

421 Turcotte DL (1997) *Fractals and chaos in geology and geophysics*. Cambridge University Press,  
422 Cambridge, (2nd Edition)

423 Turcotte DL, Malamud BD (2004) Landslides, forest fires, and earthquakes: examples of self-  
424 organized critical behavior. *Physica A*, 340: 580-589

425 van Asch TWJ, Buma J, van Beek LPH (1999) A view on some hydrological triggering systems in  
426 landslides. *Geomorphology*, 30: 25-32

427 van Asch TWJ, Malet J-P, van Beek LPH, Amisano D (2007) Techniques, issues and advances in  
428 numerical modelling of landslide hazard. *B. Soc. Géol. Fr.*, 178(2): 65–88

429 Verlet L (1967) Computer "Experiments" on Classical Fluids. I. Thermodynamical Properties of  
430 Lennard–Jones Molecules. *Physical Review*, 159: 98